ACS APPLIED MATERIALS & INTERFACES

Research Article

www.acsami.org

Transparent Slippery Surfaces Made with Sustainable Porous Cellulose Lauroyl Ester Films

Longquan Chen,*[,†,§] Andreas Geissler,[‡,§] Elmar Bonaccurso,[†] and Kai Zhang*[,‡]

[†]Center of Smart Interfaces, Technische Universität Darmstadt, Alarich-Weiss-Straße 10, D-64287 Darmstadt, Germany

[‡]Ernst-Berl-Institute for Chemical Engineering and Macromolecular Science, Technische Universität Darmstadt, Alarich-Weiss-Straße 8, D-64287 Darmstadt, Germany

Supporting Information

ABSTRACT: In recent years, liquid repellent surfaces have attracted considerable attention because of their wide array of potential applications. In the present study, slippery surfaces were fabricated using novel sustainable, nanoporous cellulose lauroyl ester (CLE) films and slippery lubrication fluid. The nanoporous CLE films were obtained after spray-coating target surfaces using a nanoparticle suspension of CLE that was prepared via nanoprecipitation. After the deposition of the slippery liquid within the porous network, the obtained slippery surfaces exhibit both excellent liquid repellency upon liquid impact and anti-icing properties (by significantly retarding the icing time). Three-dimensional droplet manipulation was also achieved on these surfaces by taking advantage of the materials' low contact angle hysteresis and low adhesion property.

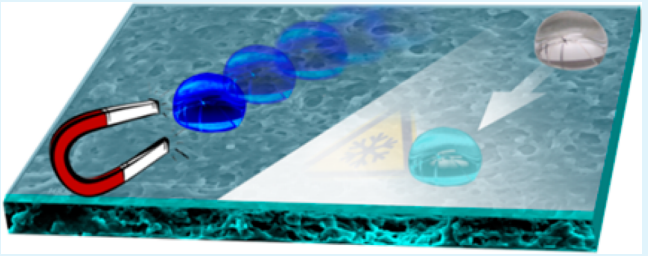

KEYWORDS: *slippery surface, porous, anti-icing, drop impact, magnetic*

1. INTRODUCTION

Driven by their robust applications, including self-cleaning coatings,[1,2] anti-fogging,[3,4] anti-icing,[5,6] heat transfer enhancement,[3,7,8] and adhesion or drag reduction in microfluidics,[9−13] liquid-repellent surfaces, such as superhydrophobic,[14−16] superomniphobic,[17,18] and superamphiphobic[19,20] surfaces, have attracted considerable attention. Generally, two types of liquid-repellent surfaces have been developed, which are inspired by natural plant surfaces. The conventional type are nano/microstructured non-wetting surfaces that mainly mimic the topography of *lotus* leaves. By entrapping air beneath a liquid drop on such surfaces, the contact area between the surface and the liquid is greatly reduced, leading to contact angles larger than 150° and sliding angles below 10°. However, the application of this type of surfaces is still limited because they become unstable under high pressure[21,22] or during drop-impact processes,[23,24] leading to the transition of the liquid from the non-wetting Cassie state[25] to the wetting Wenzel state.[26] Additionally, their non-wetting properties are compromised at low temperatures (typically, <0 °C for water) as water drops freeze or frost forms on the nano/microstructures.[27,28]

Most recently, Wong et al. reported a new type of efficient non-wetting surface, which was called a slippery liquid-infused porous surface (SLIPS).[29] This type of surface was inspired by the *Nepenthes* pitcher plant and can be fabricated by infusing a nano/microstructured porous layer with lubrication fluids, for example, perfluorinated liquids. In contrast to other nano/microstructured non-wetting surfaces, the efficient water-repellent property of SLIPS is not due to the nano/microstructures but is due to the thin film of lubricating fluid on the top of the nano/microstructured layer.[30,31] The chemical and physical homogeneity of the fluid surface results in a low contact angle hysteresis, enabling water and organic drops to roll off of the surface easily, although the contact angle is smaller than 150°. The non-wetting property of SLIPS is more stable under high pressure[29] or high temperature[32] than that of nano/microstructured non-wetting surfaces, and it has also shown remarkably low adhesion for bacteria[33,34] and ice,[29,35−37] which is promising for robust applications.

For both the conventional and new types of liquid-repellent surfaces, fabrication of rough structures with nano/micropatterns is the key step. Various materials have been used as the substrate for the fabrication of liquid-repellent surfaces. Those that are often used include silane-based compounds,[19,38] semi-fluorinated trichlorosilanes,[39] hydrophobic polymers (isotactic polypropylene),[40] and inorganic compounds.[41,42] Most recently, porous Teflon membranes, epoxy−resin-nanostructured surfaces, polypyrrole-coated aluminum, and poly(vinylidene fluoride-*co*-hexafluoropropylene) (PVDF-HFP) nanowebs were used as substrates for SLIPS.[29,35,43] In contrast to the aforementioned materials, compounds based on sustainable materials, including naturally abundant cellulose that consists of β-(1,4)-linked anhydroglucose units, have not received appropriate attention yet for use as substrate materials for liquid-repellent surfaces. A severe limitation is the hydrophilic nature of cellulose. Hence, cellulose fibers have been surface-

Received: February 5, 2014
Accepted: April 22, 2014
Published: April 22, 2014

   dx.doi.org/10.1021/am5020343 | ACS Appl. Mater. Interfaces 2014, 6, 6969−6976

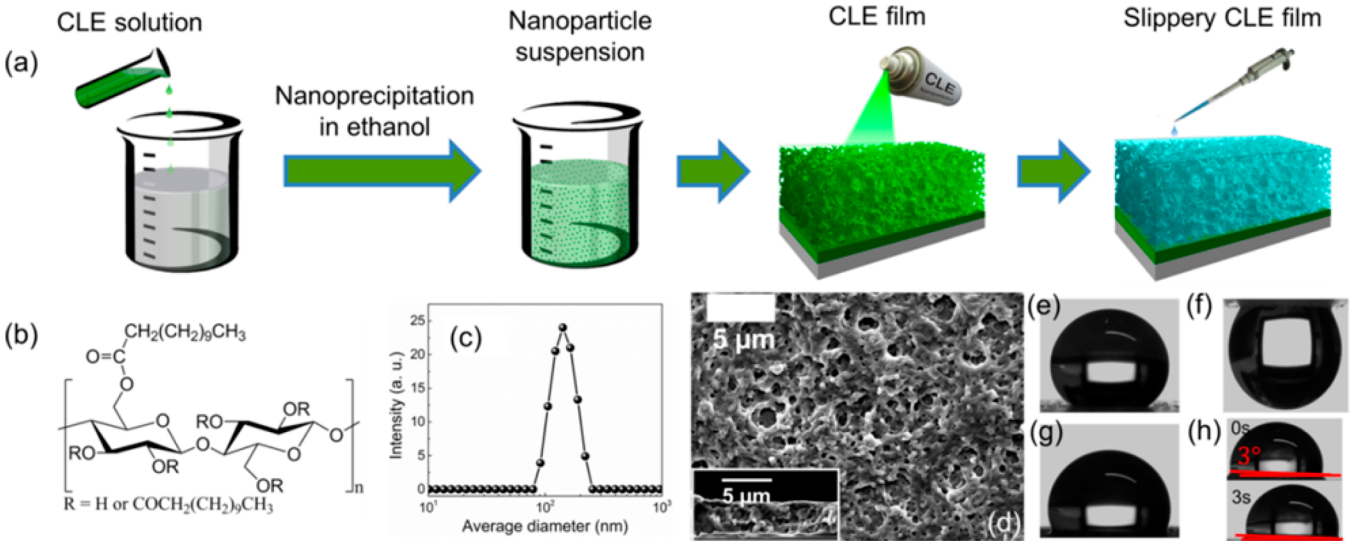

Figure 1. (a) Schematic illustration of the fabrication process of slippery cellulose lauroyl ester (CLE) surfaces. (b) Schematic representation of the chemical structure of CLE. (c) Dynamic light scattering (DLS) curve of CLE nanoparticles. (d) Scanning electron microscope (SEM) images of the nanoporous CLE film. The inset shows the side profile of the film. (e) Photograph of a 5 μL water drop on the nanoporous CLE film. (f) Shape of the drop on the nanoporous CLE film when it was turned upside down. (g) Photograph of a 5 μL water drop on the slippery CLE film after the infusion of perfluoropolyether into the nanoporous CLE film. (h) Sliding of a 5 μL water drop on the slippery CLE film.

hydrophobized (e.g., using synthetic polymers[44,45] or perfluorinated compounds[46,47]) to produce cellulose-based superhydrophobic or superamphiphobic surfaces. However, further applications of such cellulose fibers are still limited because of their high surface roughness and the non-solubility of cellulose in common solvents.

Thus, the development of robust liquid-repellent surfaces using sustainable materials via simple fabrication methods is of fundamental interest for research and industrial applications. In this article, we report a simple, fast, and reproducible method that is easily scalable to large and irregular areas for fabricating transparent slippery surfaces based on nanoporous films of sustainable cellulose lauroyl ester (CLE) via spray-coating. These slippery surfaces are liquid-repellent for water, ionic liquids, and some organic liquids such as glycerol. They also showed excellent liquid repellency upon liquid impact and outstanding anti-icing properties. Using these surfaces, we further demonstrate that their small contact angle hysteresis and low adhesion enable the 3D manipulation of drops by applying external magnetic forces. In addition, the fabrication of slippery surfaces using CLE is not limited by the size or the geometry of the surface because spray-coating is a very generally applicable coating technique.

2. RESULTS AND DISCUSSION

CLE containing sustainable cellulose and lauroyl groups (Figure 1b) with a degree of substitution of 3 according to elemental analysis and a number-averaged degree of polymerization (DP_n) of 102 was synthesized after the total esterification of hydroxyl groups on the cellulose backbone (Supporting Information Scheme S1 and Figures S1 and S2). CLE is highly soluble in non-polar solvents including tetrahydrofuran (THF), toluene, and dichloromethane. A target surface, for example, glass or silicon wafer, was initially dip-coated in a 10 mg/mL CLE solution in toluene, resulting in a flat CLE layer of 76 ± 3 nm according to ellipsometry measurements. The layer was hydrophobic and exhibited a water contact angle of 101 ± 2° (Supporting Information Figure S3). The thickness of the CLE layer can be varied by using CLE solutions of different concentrations. The CLE layer was completely transparent (Supporting Information Figure S4) and was used as an adhesion layer between the target surface and nanoporous film. Subsequently, the target surfaces coated with the CLE layer were spray-coated with CLE nanoparticles dispersed in ethanol (Figure 1a). The nanoparticles were fabricated from the CLE solution via nanoprecipitation, they had an average diameter of 140 ± 1 nm, and they showed a narrow size distribution (PDI = 0.04 ± 0.02) (Figure 1c). After the evaporation of ethanol, a nanostructured CLE film was formed. This CLE film was composed of a porous network consisting of aggregated CLE and pores on the nano/microscale (Figure 1d). The individual pores had diameters between 30 and 1060 nm (Supporting Information Figure S5). No individual CLE nanoparticles were observed on these porous CLE films. Therefore, CLE nanoparticles must have coalesced during the evaporation of the solvent and formed a nanoporous film (Figure 1d). In comparison, nanoparticles from cellulose stearoyl esters (CSE) can be maintained as individual nanoparticles after spraying onto a target surface.[48] After nanoprecipitation from the CSE solution into water and removal of the solvents, the stearoyl groups within CSE nanoparticles can form stable crystalline regions and support the formation of individual nanoparticles. However, the crystallization feasibility of lauroyl groups is much lower because of the short alkane chain length, so no stable crystalline structure could be formed to stabilize the individual nanoparticles. After spraying and drying, the CLE nanoparticles used in the present study coalesced at the nanoparticle surface. Subsequently, only a porous network of CLE was obtained.

The porous CLE film showed increased hydrophobicity and a water contact angle of 140 ± 1° (Figure 1e). The sliding angle measurement indicated that the drop stayed in the Wenzel wetting state,[26] as it remained stuck on the surface for tilting angles up to 180° (Figure 1f). Although the nanoporous CLE film is highly hydrophobic under static wetting conditions, the

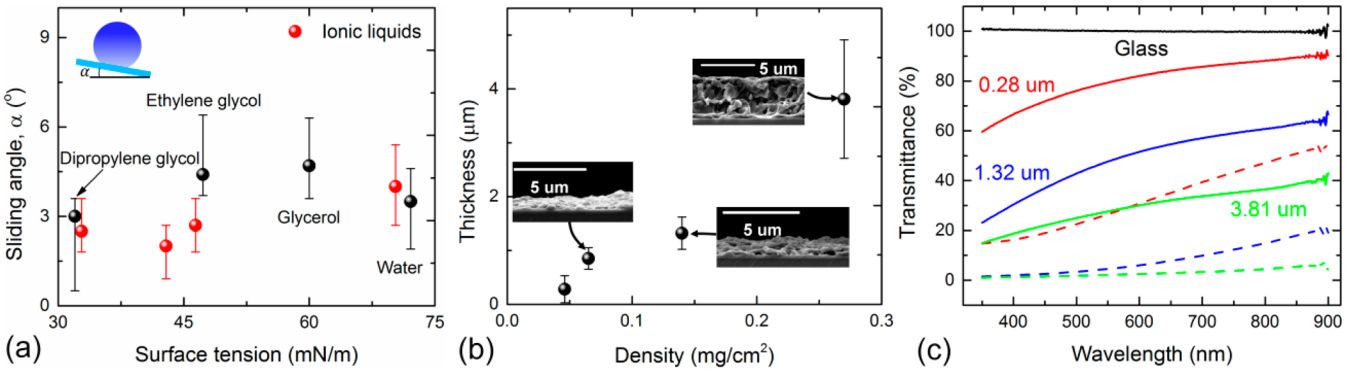

Figure 2. (a) Sliding angle of slippery CLE films as a function of surface tension for various liquids (properties are listed in Supporting Information Table S1). (b) Thickness of nanoporous CLE films as a function of the density on a target surface. (c) Transparency of various nanoporous CLE films (dotted lines) and corresponding slippery CLE films (solid lines).

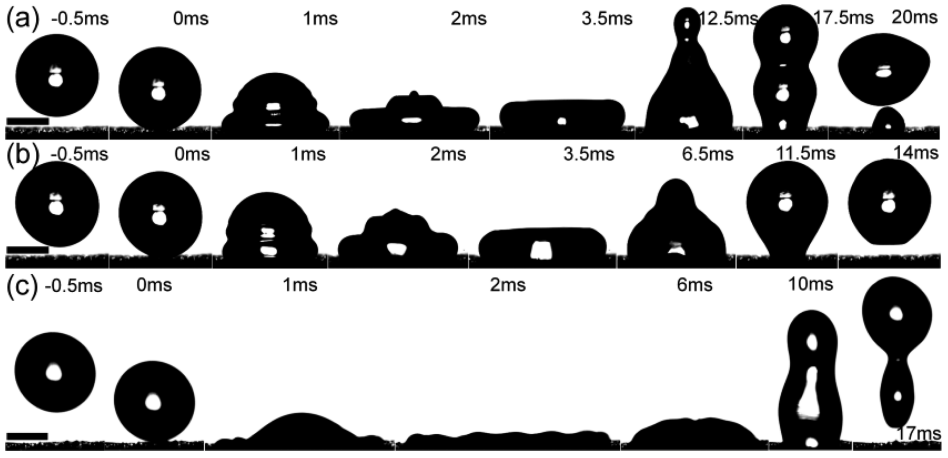

Figure 3. Water droplet (5 μL) impinging on the nanoporous CLE film with a critical speed of 0.5 m/s (a) and on the perfluoropolyether-infused slippery CLE film with critical speeds of 0.5 m/s (b) and 1.5 m/s (c). The scale bar is 1 mm.

use of this film is limited because of its high adhesion property for liquids.

The liquid repellency of the porous CLE film was improved by infusing it with perfluoropolyether as a lubrication film. Perfluoropolyether is immiscible with most organic solvents and has very low volatility. Moreover, perfluoropolyether is compatible with various plastomers, elastomers, and most metals over a wide temperature range.[49] The perfluoropolyether-infused slippery CLE films showed a water contact angle of 112 ± 1° (Figure 1g), which is smaller than that on bare nanoporous CLE films. However, because of the extremely small roughness and the chemical homogeneity of the liquid surface, the contact angle hysteresis of water was only 2°, and a 5 μL water drop can slide down from the surface with a tilting angle as low as 3° (Figure 1h). The sliding angles for various organic liquids and ionic liquids were also measured (Figure 2a). For these liquids, with surface tensions down to 33 mN/m and viscosities up to 1.4 Pas, the sliding angles were all between 2 and 6°. Hence, the slippery CLE films can be considered superomniphobic.

The bare nanoporous CLE films were semi-transparent (Figure 2c) because of the diffuse reflectance of light by the porous structures. When a lubrication film was infused, the transparency of the surface increased by at least a factor of 2 (Figure 2c). In addition, the transparency of the surfaces can be tuned by controlling the thickness of the nanoporous CLE film. A film thickness between 0.28 and 3.81 μm was obtained with a CLE density of 0.046−0.270 mg/cm^2 (Figure 2b). Subsequently, the visible-light transparency of the slippery CLE films was tuned to between 30 and 80%, whereas the liquid repellency remained the same. Such transparent liquid-repellent coatings can be promising candidates for solar cell applications,[50] where the self-cleaning coatings can improve the collection efficiency of sunlight (washing away dirt and dust) and need to be highly transparent.[14,51,52]

In practical applications, the impingement of droplets on surfaces often occurs and hence it is important to study the dynamic wetting of the surfaces.[14,19,24,53] Figure 3a shows a 5 μL water drop impacting on the porous CLE film with a speed V = 0.5 m/s. The kinetic energy of the impacting drop was transferred into surface energy during spreading. After the drop reached its maximum spreading area, it started to recoil. However, the penetration of the liquid into the porous structures resulted in a large adhesion, leading to the drop sticking to the surface (Figure 3a and Supporting Information Movie S1). Eventually, the drop did not bounce off of the surface completely and was torn apart after 20 ms. Similar phenomena were observed for any other impact speeds. In contrast, we found that the drops rebounded from the slippery surfaces for impacting speeds equal to or larger than a critical value V_c of 0.5 m/s (Figure 3b,c and Supporting Information Movies S2 and S3). This critical speed can be estimated by balancing the energy terms during spreading. For a drop of radius R, the kinetic energy of impact is estimated as $\rho R^3 V^2$,

dx.doi.org/10.1021/am5020343 | ACS Appl. Mater. Interfaces 2014, 6, 6969−6976

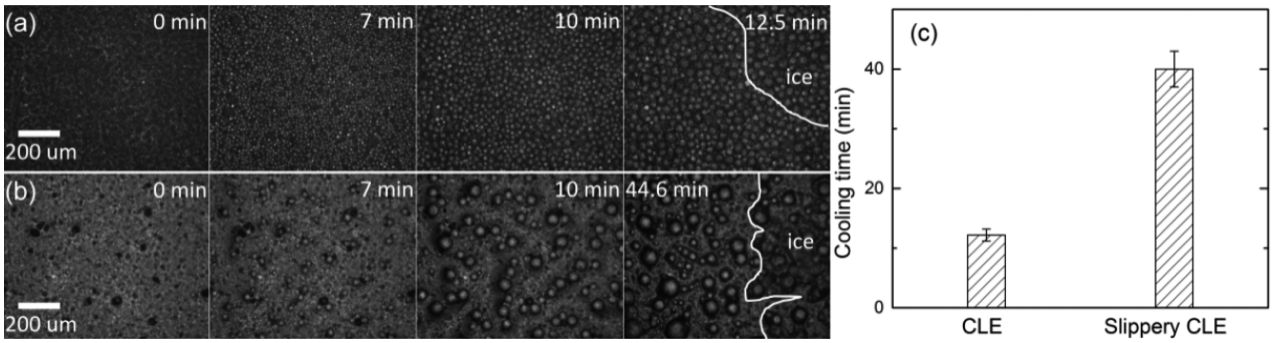

Figure 4. Ice/frost formation on the nanoporous CLE film (a) and slippery CLE film (b). (c) Cooling time until the ice/frost formation on the two films.

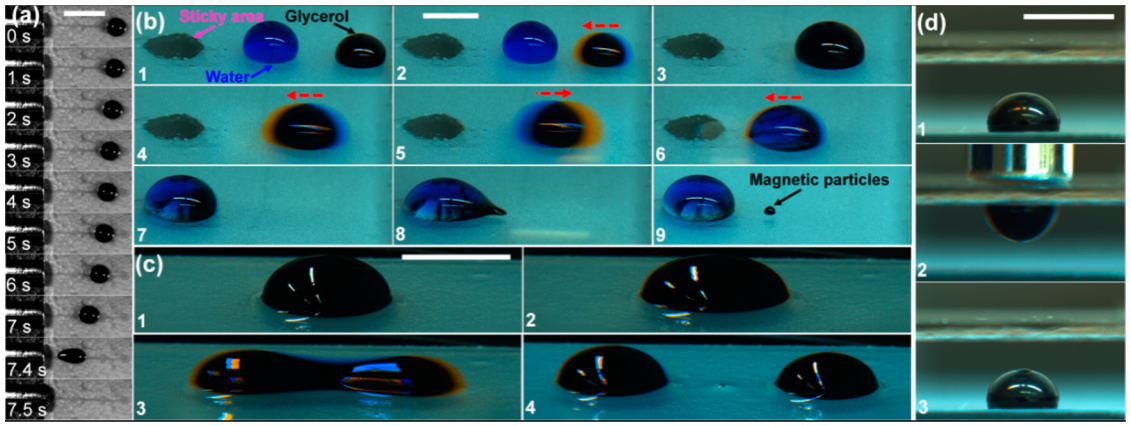

Figure 5. (a) Horizontal movement of a 25 μL magnetic glycerol drop by a normal magnet (the magnet is on the left). The magnetic field is 0.06 T. The scale bar is 10 mm. (b) Magnetic glycerol drop (25 μL) moved by the magnetic field to a 30 μL water drop. After coalescing, the two liquids were mixed by "shaking" the drops, and the mixed drop was moved to a sticky area. Eventually, the magnetic particles were removed from the mixed drop by the magnet. (c) Magnetic glycerol drop (60 μL) divided into two droplets by two magnets applied beside the drop. (d) Magnetic glycerol drop (15 μL) transferred from a lower to an upper surface and back by a moving magnet. The scale bar in panels b–d is 5 mm.

where ρ is the density of the drop. This energy is converted into surface energy during the spreading stage and is released during the recoiling stage. The main energy resisting retraction is the free energy of adhesion, which scales as $R^2\gamma(1 + \cos\theta)$,[54] where γ is the surface tension of the drop and θ is the equilibrium contact angle (here, 112° for water). The drop can bounce off of the surface only when its kinetic energy is larger than its adhesion free energy (i.e., the impinging speed must be larger than a critical value, $V > V_c = ((\gamma(1 + \cos\theta))/(\rho R))^{1/2}$). The critical speed of 0.5 m/s for rebounding drops observed in the experiments is very close to the theoretical value of 0.2 m/s. For naturally impinging raindrops, the terminal velocity is around 6 m/s (for 3 mm diameter raindrops).[55] Therefore, it is possible to use our slippery CLE films in outdoor applications such as windshields.

Outdoor applications of liquid-repellent surfaces in low-temperature environments also require the surfaces to be non-wetting or anti-icing. Indeed, Wong et al. have shown that ice adhesion to SLIPS is very low.[29,35] Here, we demonstrate that the slippery CLE films also delay ice formation. Figure 4a,b shows the icing process on the nanoporous CLE film and the slippery CLE film on silicon substrates (20 mm × 20 mm × 500 μm), which were cooled from 22 to −10°C. The relative humidity was 45 ± 3%. Micron-sized water drops were observed on both surfaces after ∼3 min of cooling when the temperature was lower than the dew point (∼8 °C[56]). On the nanoporous CLE film, the average size of the water drops grew with time because of the growth of each condensate drop and the coalescence of neighbor drops.[3] The condensate drops on the slippery CLE film were very movable because of low contact angle hysteresis.[35] Most drops coalesced, and the coalesced drop moved out of the field of view. Eventually, the surface coverage of the drops on the slippery CLE film was less than that on the nanoporous CLE film (Figure 4). Ice crystals nucleated on the nanoporous CLE film after 12 ± 1 min of cooling (Figure 4a,d). A similar cooling time has been observed on superhydrophobic surfaces.[57] In contrast, on the slippery CLE film, ice nucleation started only after 40 ± 3 min of cooling, thus delaying the icing time by a factor of approximately four (Figure 4c,d). Moreover, it took only 41 ± 5 s for all of the drops in the field of view on the nanoporous CLE film to freeze, whereas this process took 150 ± 10 s on the slippery CLE film. In summary, we found that ice nucleation on the slippery films was significantly delayed compared to that on other (super)hydrophobic films.

In recent years, superhydrophobic surfaces have been used in microfluidic devices because they show reduced adhesion and friction with liquids.[9−13] Only a small drag force is required in order for the liquid/drop to be moved easily by small external forces. Here, we show that some essential processes required for microfluidic applications, including transport, mixing, or the breaking of a larger droplet into smaller ones, can be achieved on the slippery CLE films using external forces. Figure 5a shows a 25 μL glycerol drop containing 0.5 wt % of magnetic

microparticles (iron oxide particles with a size of 5 μm) moving on the slippery CLE film under magnetic actuation. The magnet bar was placed on the left side, and the magnetic glycerol drop was deposited on the right side of the surface. The critical magnetic field required to start the drop in motion was 0.06 T (measured at a 20 mm drop−magnet distance by a Teslameter, Projekt Elektronik GmbH, Berlin). In contrast, the same drop could not be moved with the same magnetic field on the nanoporous CLE film because the adhesion was too large. Under the action of the magnetic field, the drop accelerated and hit the magnet after 7.4 s. The minimum magnetic field/force and the speed of the moving drops depend on the mass of the drop and the concentration of the magnetic particles.

In many applications, including regenerative medicine and biointerfacial engineering, the control via magnetic actuation (i.e., the movement and mixing of diverse liquids under the control of a magnetic field as well as the separation of magnetic particles from liquids) is of particular interest.[58,59] Using magnetic actuation on the slippery CLE film, we further demonstrated controlled mixing (Figure 5b and Supporting Information Movie S4), drop breakup (Figure 5c and Supporting Information Movie S5), and separation of magnetic particles from liquids. A 25 μL glycerol drop containing magnetic particles (the drop is black because of the magnetic particles) was moved by the magnet, placed below the substrate, to a 30 μL water drop (colored blue). After the coalescence, the resulting drop became black as the water drop was engulfed at first by the glycerol drop because of the surface tension difference (image 3 in Figure 5b). Then, the merged drop was "shaken" by shuffling the magnet bar horizontally underneath the substrate (image 4−6 in Figure 5b). Once the two liquids were well-mixed, the merged drop was moved by the magnet to a sticky circular area without CLE film (image 6 in Figure 5b). Because of the larger adhesion of the liquid to the sticky area, the magnetic particles could be extracted from the drop by the magnet (images 8 and 9 in Figure 5b and Movie S4). The extraction of magnetic particles was very effective, as more than 98 ± 1 wt % of the magnetic particles were removed under magnetic actuation (Supporting Information Figure S6).

By positioning two magnets on two opposite sides of a 60 μL glycerol drop containing magnetic particles and placing the drop on a horizontal CLE substrate, the drop could be broken into two smaller drops (Figure 5c). The motion of the drops could be controlled not only in a plane (i.e., in two dimensions) but also perpendicular to the substrate. Figure 5d shows the transfer of a magnetic glycerol drop between two slippery surfaces that are vertically separated by 4 mm. Once the magnet approached the top surface, the drop sitting on the bottom surface jumped upward and was completely transferred to the top surface. When the magnet was moved away, the drop fell back onto the bottom surface under the action of gravity. Most recently, Timonen et al. and others reported reversible manipulation of magnetic droplets on superhydrophobic surfaces.[60,61] Here, we demonstrated that the reversible switching of magnetic droplets is also feasible on slippery surfaces. In summary, we showed that some standard processes for microfluidic applications can be easily achieved on slippery CLE substrates and that drop actuation can be carried out in three dimensions. Nevertheless, a cloaking layer might form on the droplet if the spreading coefficient is larger than zero,[31] which can lead to contamination of the samples.

The spray-coating technique used in the present study has many advantages, such as universal applicability, simple experimental apparatus, compatibility with ambient air conditions, and avoidance of hazardous solvents, in comparison to other methods including electrochemical deposition,[15] plasma etching,[29] chemical vapor deposition,[14,19,53] or electrospinning.[17] A further advantage of spray-coating is that the coating is not limited by the size and shape of the target surface. For instance, highly curved or not easily accessible objects such as the inner side of bottles could be spray-coated with slippery CLE films (Figure 6a). In the literature, many methods for the fabrication of liquid-repellent surfaces, such as plasma etching[29] and chemical vapor deposition,[14,19,53] have been carried out under extreme pressure or temperature conditions. In contrast, the slippery CLE film can be sprayed on objects that do not withstand high temperature, for example, plastic and paper (Figure 6b). By impacting the slippery surface via 100 mL water drops from a height of 50 cm, the surface still maintained its low adhesion (Supporting Information Movie S6). Moreover, damaged or scratched surfaces can be repeatedly and conveniently repaired by applying multiple spray-coatings.

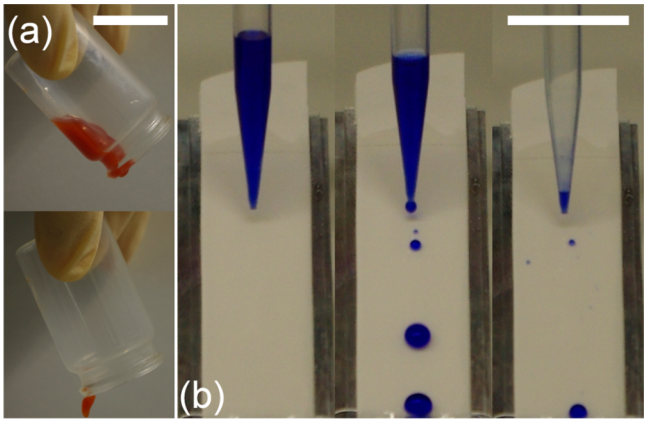

Figure 6. Representative demonstrations of a small bottle (a) and a piece of paper (b) after spray-coating with slippery CLE films (the paper sample that was directly infused with slippery liquid was still wettable, as shown in Supporting Information Figure S7). The red squishy liquid in panel a is tomato ketchup, and the blue liquid in panel b is water containing dye. The scale bars are 2.0 mm.

3. CONCLUSIONS

In summary, transparent slippery substrates were fabricated by spray-coating nanoparticle suspensions of sustainable cellulose lauroyl ester (CLE) that were subsequently infused with a perfluorinated lubrication liquid. The slippery CLE films exhibited very low adhesion for static and dynamic wetting processes and also showed good anti-icing properties by significantly retarding the ice-formation process at −10 °C under ambient conditions. The low adhesion and friction between the coating and various liquids enable 3D drop manipulation via magnetic actuation, as required for open microfluidic applications. Because the spray-coating technique is simple, fast, and scalable to large and irregular areas, the slippery CLE film is promising for use in many applications such as the coating of car windows, solar cell panels, and microfluidic devices.

4. EXPERIMENTAL SECTION

Materials. Microcrystalline cellulose (MCC) with a granule size of 50 μm, lauroyl chloride (98%), perfluoropolyether (Fomblin®Y, lot no. MKBJ7302V), glycerol, ethylene glycol, dipropylene glycol, and magnetic iron oxide particles with a size of 5 μm were received from Sigma-Aldrich (Steinheim, Germany). The four ionic liquids were 1-butyl-3-methylimidazolium iodide, 1-butyl-3-methylimidazolium bis-(trifluoromethylsulfonyl)imide, 1-butyl-3-methylimidazolium tetrafluoroborate, and 2-hydroxyethylammonium formate (io-li-tech GmbH, Germany). Other chemicals were all of analytical grade and used as received. Deionized (DI) water was used in all experiments.

Synthesis of Cellulose Lauroyl Ester (CLE). In a typical case, 1 g of cellulose was washed with methanol and pyridine to remove traces of moisture before it was suspended in 30 mL of pyridine. Under stirring, the mixture was heated to 100 °C. Then, 8.96 mL of lauroyl chloride (98%) (2 mol per mol OH of AGUs) was dropped to the hot suspension while the system was purged with nitrogen. After 1 h of stirring at 100 °C, the reaction mixture was poured (still hot) into 200 mL of ethanol, and the precipitate was separated by centrifugation. The product was purified via repeating dissolution in dichloromethane and precipitation in five volumes ethanol. Lastly, the product was dried under vacuum. Yield: 4.3 g.

Nanoprecipitation of CLE. CLE was transformed into nanoparticles via nanoprecipitation through a dropping technique.[62] Before nanoprecipitation, CLE was dissolved in tetrahydrofuran (THF) at a typical concentration of 10 mg/mL. The solution was filtered with a glass fiber filter with a pore size of 1 μm under vacuum. Then, 50 mL of CLE solution was pipetted drop-by-drop into 250 mL of ethanol under vigorous stirring at room temperature, and the obtained suspension of CLE nanoparticles was used for further spray-coating.

Fabrication of Slippery Surface. Glass slides, standard microscope slides (made of soda-lime glass, 76 × 26 mm^2, Carl-Roth GmbH, Karlsruhe, Germany), silicon wafers (20 mm × 20 mm × 500 μm, Crys Tec GmbH, Germany), and coverslips (24 × 24 mm^2, Carl-Roth) were dip-coated using a 10 mg/mL CLE solution in toluene at a coating velocity of 2 mm/s and were dried under air. Then, these surfaces were spray-coated using CLE-NPs in ethanol. Spray-coating was carried out using an airbrush (model Colani) from Harder & Steenbeck GmbH & Co. KG (Norderstedt, Germany) at a pressure of 4 bar and a distance of 25 cm under air. After that, 1−15 μL (depending on the area of the coating surface and the thickness of the CLE film) of perfluoropolyether was deposited on the CLE layer so that the volume of the liquid was approximately 1.5 volumes of the porous layer. The slippery surfaces were obtained after the perfluoropolyether completely sank into the CLE film.

Magnetic Glycerol. Fifty milligrams of iron oxide was put into 10 g of glycerol. They were mixed by 5 min before the experiment.

Characterization. *Elemental Analysis.* The content of carbon, hydrogen, and nitrogen was determined with a Vario EL III CHN elemental analyzer from Elementar (Hanau, Germany). The total degree of substitution ascribed to lauroyl groups (DS_{LE}) was calculated on the basis of[63]

$$DS_{SE} = \frac{5.13766 - 11.5592 \times C\%}{0.996863 \times C\% - 0.856277 \times 12 + 12 \times C\%} \quad (1)$$

where C% is the determined content of carbon.

Dynamic Light Scattering (DLS). DLS measurements were performed on a Zetasizer Nano ZS (Malvern Instruments Ltd., UK) using a 4 mW He−Ne laser with a 633 nm wavelength incident beam. Then, the nanoparticle suspension was diluted with ethanol to a concentration of ∼0.04 mg/mL, and 1 mL of the suspension in quartz cuvette (Type 3, from Starna GmbH, Pfungstadt, Germany) was used for the size measurement. The measurement was repeated three times for 10 runs with 10 s per measurement.

Scanning Electron Microscopy (SEM). SEM images were obtained on a Philips XL30 FEG high-resolution scanning electron microscope (HR-SEM) (FEI Deutschland GmbH, Frankfurt/Main, Germany). A 3 nm layer of platinum/palladium was coated on the surface of the samples before SEM measurements.

Optical Transmission Measurement. Optical transmission measurements were carried out on Varian Cary 50 UV−vis spectrophotometer (Agilent Technologies Deutschland GmbH, Böblingen, Germany) between the wavelengths of 350 and 900 nm.

Drop Impact Experiments. Drop impact experiments were obtained using a high-speed camera at 20 000 fps. The magnetic field was measured with a Teslameter (Projekt Elektronik GmbH, Berlin).

Icing Experiments. Icing experiments were carried out on air-cooled thermoelectric cold plates (AHP-1200CAS series) under room environmental conditions. The relative humidity was 45 ± 3%, and the room temperature was 22 ± 2 °C. Surfaces were put on the cooling plate and were cooled from 22 to −10 °C, which took around 10 min. The condensation and icing process was recorded from the top view using a low-speed CCD camera (1 fps, Pixelink PL-531MU, 1280 × 1024 pixel) for 1 h.

■ ASSOCIATED CONTENT

Ⓢ Supporting Information

FTIR and FT Raman spectra, ellipsometry, size-exclusion chromatography, pore size distribution, and 7 movie files. This material is available free of charge via the Internet at http://pubs.acs.org.

■ AUTHOR INFORMATION

Corresponding Authors

*(L.C.) E-mail: l.chen@csi.tu-darmstadt.de.

*(K.Z.) E-mail: zhang@cellulose.tu-darmstadt.de.

Author Contributions

§L.C. and A.G. contributed equally to this work. The manuscript was written through contributions of all authors. All authors have given approval to the final version of the manuscript.

Notes

The authors declare no competing financial interest.

■ ACKNOWLEDGMENTS

This research was supported by the German Research Foundation (DFG) within the Cluster of Excellence 259 "Smart Interfaces − Understanding and Designing Fluid Boundaries" (L.C. and E.B.). A.G. and K.Z. thank the Hessian excellence initiative LOEWE, research cluster Soft Control, for financial support. K.Z. thanks Prof. Markus Biesalski for the kind support.

■ REFERENCES

(1) Wisdom, K. M.; Watson, J. A.; Qu, X.; Liu, F.; Watson, G. S.; Chen, C. H. Self-Cleaning of Superhydrophobic Surfaces by Self-Propelled Jumping Condensate. *Proc. Natl. Acad. Sci. U.S.A.* **2013**, *110*, 7992−7997.

(2) Nishimoto, S.; Bhushan, B. Bioinspired Self-Cleaning Surfaces with Superhydrophobicity, Superoleophobicity, and Superhydrophilicity. *RSC Adv.* **2013**, *3*, 671−690.

(3) Boreyko, J. B.; Chen, C. H. Self-Propelled Dropwise Condensate on Superhydrophobic Surfaces. *Phys. Rev. Lett.* **2009**, *103*, 184501-1−184501-4.

(4) Chen, X. M.; Wu, J.; Ma, R. Y.; Hua, M.; Koratkar, N.; Yao, S. H.; Wang, Z. K. Nograssed Micropyramidal Architectures for Continuous Dropwise Condensation. *Adv. Funct. Mater.* **2011**, *21*, 4617−4623.

(5) Guo, P.; Zheng, Y.; Wen, M.; Song, C.; Lin, Y.; Jiang, L. Icephobic/Anti-Icing Properties of Micro/Nanostructured Surfaces. *Adv. Mater.* **2012**, *24*, 2642−2648.

(6) Stone, H. A. Ice-Phobic Surfaces That Are Wet. *ACS Nano* **2012**, *6*, 6536−6540.

(7) Xiao, R.; Miljkovic, N.; Enright, R.; Wang, E. N. Immersion Condensation on Oil-Infused Heterogeneous Surfaces for Enhanced Heat Transfer. *Sci. Rep.* **2013**, *3*, 1988-1−1988-6.
(8) Li, C.; Wang, Z.; Wang, P. I.; Peles, Y.; Koratkar, N.; Peterson, G. P. Nanostructured Copper Interfaces for Enhanced Boiling. *Small* **2008**, *4*, 1084−1088.
(9) Daniello, R. J.; Waterhouse, N. E.; Rothstein, J. P. Drag Reduction in Turbulent Flows over Superhydrophobic Surfaces. *Phys. Fluids* **2009**, *21*, 085103-1−085103-9.
(10) Truesdell, R.; Mammoli, A.; Vorobieff, P.; van Swol, F.; Brinker, C. J. Drag Reduction on a Patterned Superhydrophobic Surface. *Phys. Rev. Lett.* **2006**, *97*, 044504-1−044504-4.
(11) Choi, C.; Kim, C. Large Slip of Aqueous Liquid Flow over a Nanoengineered Superhydrophobic Surface. *Phys. Rev. Lett.* **2006**, *96*, 066001-1−066001-4.
(12) Koc, Y.; de Mello, A.; McHale, G.; Newton, M.; Roach, P.; Shirtcliffe, N. Nano-Scale Superhydrophobicity: Suppression of Protein Adsorption and Promotion of Flow-Induced Detachment. *Lab Chip* **2008**, *8*, 582−586.
(13) Roach, P.; Farrar, D.; Perry, C. Surface Tailoring for Controlled Protein Adsorption: Effect of Topography at the Nanometer Scale and Chemistry. *J. Am. Chem. Soc.* **2006**, *128*, 3939−3945.
(14) Deng, X.; Mammen, L.; Zhao, Y.; Lellig, P.; Müllen, K.; Li, C.; Butt, H.-J.; Vollmer, D. Transparent, Thermally Stable and Mechanically Robust Superhydrophobic Surfaces Made from Porous Silicia Capsules. *Adv. Mater.* **2011**, *23*, 2962−2965.
(15) Lai, Y.; Gao, X.; Zhuang, H.; Huang, J.; Lin, C.; Jiang, L. Designing Superhydrophobic Porous Nanostructures with Tunable Water Adhesion. *Adv. Mater.* **2009**, *21*, 3799−3803.
(16) Feng, X.; Jiang, L. Design and Creation of Superwetting/Antiwetting Surfaces. *Adv. Mater.* **2006**, *18*, 3063−3078.
(17) Pan, S.; Kota, A.; Mabry, J.; Tuteja, A. Superomniphobic Surfaces for Effective Chemical Shielding. *J. Am. Chem. Soc.* **2013**, *135*, 578−581.
(18) Kobaku, S.; Kota, A.; Lee, D.; Mabry, J.; Tuteja, A. Patterned Superomniphobic-Superomniphilic Surfaces: Templates for Site-Selective Self-Assembly. *Angew. Chem., Int. Ed.* **2012**, *51*, 10109−10113.
(19) Deng, X.; Mammen, L.; Butt, H.-J.; Vollmer, D. Candle Soot as a Template for a Transparent Robust Superamphiphobic Coating. *Science* **2012**, *335*, 67−70.
(20) Zhou, H.; Wang, H.; Niu, H.; Gestos, A.; Lin, T. Robust, Self-Healing Superamphiphobic Fabrics Prepared by Two-Step Coating of Fluoro-Containing Polymer, Fluoroalkyl Silane, and Modified Silica Nanoparticles. *Adv. Funct. Mater.* **2013**, *23*, 1664−1670.
(21) Poetes, R.; Holtzmann, K.; Franze, K.; Steiner, U. Metastable Underwater Superhydrophobicity. *Phys. Rev. Lett.* **2010**, *105*, 166104-1−166104-4.
(22) Papadopoulos, P.; Mammen, L.; Deng, X.; Vollmer, D.; Butt, H. How Superhydrophobicity Breaks Down. *Proc. Natl. Acad. Sci. U.S.A.* **2013**, *110*, 3254−3258.
(23) Koishi, T.; Yasuoka, K.; Fujikawa, S.; Ebisuzaki, T.; Zeng, X. Coexistence and Transition between Cassie and Wenzel State on Pillared Hydrophobic Surface. *Proc. Natl. Acad. Sci. U.S.A.* **2009**, *106*, 8435−8440.
(24) Deng, T.; Varanasi, K.; Hsu, M.; Bhate, N.; Keimel, C.; Stein, J.; Blohm, M. Nonwetting of Impinging Droplets on Textured Surfaces. *Appl. Phys. Lett.* **2009**, *94*, 133109-1−133109-3.
(25) Cassie, A. B. D.; Baxter, S. Wettability of Porous Surfaces. *Trans. Faraday Soc.* **1944**, *40*, 546−551.
(26) Wenzel, R. N. Resistance of Solid Surfaces to Wetting by Water. *Ind. Eng. Chem.* **1936**, *28*, 988−994.
(27) He, M.; Li, H.; Wang, J.; Song, Y. Superhydrophobic Surface at Low Surface Temperature. *Appl. Phys. Lett.* **2011**, *98*, 093118-1−093118-3.
(28) Varanasi, K.; Deng, T.; Smith, J.; Hsu, M.; Bhate, N. Frost Formation and Ice Adhesion on Superhydrophobic Surfaces. *Appl. Phys. Lett.* **2010**, *97*, 234102-1−234102-3.
(29) Wong, T. S.; Kang, S. H.; Tang, S. K. Y.; Smythe, E. J.; Hatton, B. D.; Grinthal, A.; Aizenberg, J. Bioinspired Self-Repairing Slippery Surfaces with Pressure-Stable Omniphobicity. *Nature* **2011**, *477*, 443−447.
(30) Quere, D. Non-Sticking Drops. *Rep. Prog. Phys.* **2005**, *68*, 2495−2532.
(31) Smith, J. D.; Dhiman, R.; Anand, S.; Reza-Garduno, E.; Cohen, R. E.; McKinley, G. H.; Varanasi, K. K. Droplet Mobility on Lubricant-Impregnated Surfaces. *Soft Matter* **2013**, *9*, 1772−1780.
(32) Daniel, D.; Mankin, M. N.; Belisle, R. A.; Wong, T. S.; Aizenberg, J. Lubricant-Infused Micro/Nano-Structured Surfaces with Tunable Dynamic Omniphobicity at High Temperatures. *Appl. Phys. Lett.* **2013**, *102*, 231603-1−231603-4.
(33) Epstein, A. K.; Wong, T. S.; Belisle, R. A.; Boggs, E. M.; Aizenberg, J. Liquid-Infused Structured Surfaces with Exceptional Anti-Biofouling Performance. *Proc. Natl. Acad. Sci. U.S.A.* **2012**, *109*, 13182−13187.
(34) Vogel, N.; Belisle, R. A.; Hatton, B.; Wong, T. S.; Aizenberg, J. Transparency and Damage Tolerance of Patternable Omniphobic Lubricated Surfaces Based on Inverse Colloidal Monolayers. *Nat. Commun.* **2013**, *4*, 2176.
(35) Kim, P.; Wong, T. S.; Alvarenga, J.; Kreder, M. J.; Adorno-Martinez, W. E.; Aizenberg, J. Liquid-Infused Nanostructured Surfaces with Extreme Anti-Ice and Anti-Frost Performance. *ACS Nano* **2012**, *6*, 6569−6577.
(36) Subramanyam, S. B.; Rykaczewski, K.; Varanasi, K. K. Ice Adhesion on Lubricant-Impregnated Textured Surfaces. *Langmuir* **2013**, *29*, 13414−13418.
(37) Anand, S.; Paxson, A. T.; Dhiman, R.; Smith, J. D.; Varanasi, K. K. Enhanced Condensation on Lubricant-Impregnated Nanotextured Surfaces. *ACS Nano* **2012**, *6*, 10122−10129.
(38) Dorrer, C.; Rühe, J. Wetting of Silicon Nanograss: From Superhydrophilic to Superhydrophobic Surfaces. *Adv. Mater.* **2008**, *20*, 159−163.
(39) Genzer, J. Creating Long-Lived Superhydrophobic Polymer Surfaces through Mechanically Assembled Monolayers. *Science* **2000**, *290*, 2130−2133.
(40) Erbil, H. Y.; Demirel, A. L.; Avci, Y.; Mert, O. Transformation of a Simple Plastic into a Superhydrophobic Surface. *Science* **2003**, *299*, 1377−1380.
(41) Guo, Z.; Zhou, F.; Hao, J.; Liu, W. Stable Biomimetic Super-Hydrophobic Engineering Materials. *J. Am. Chem. Soc.* **2005**, *127*, 15670−15671.
(42) Yao, X.; Chen, Q.; Xu, L.; Li, Q.; Song, Y.; Gao, X.; Quéré, D.; Jiang, L. Bioinspired Ribbed Nanoneedles with Robust Super-hydrophobicity. *Adv. Funct. Mater.* **2010**, *20*, 656−662.
(43) Lalia, B. S.; Anand, S.; Varanasi, K. K.; Hashaikeh, R. Fog-Harvesting Potential of Lubricant-Impregnated Electrospun Nano-mats. *Langmuir* **2013**, *29*, 13081−13088.
(44) Nystrom, D.; Lindqvist, J.; Ostmark, E.; Hult, A.; Malmstrom, E. Superhydrophobic Bio-Fibre Surfaces via Tailored Grafting Architecture. *Chem. Commun.* **2006**, 3594−3596.
(45) Roy, D.; Guthrie, J. T.; Perrier, S. Graft Polymerization: Grafting Poly(styrene) from Cellulose via Reversible Addition−Fragmentation Chain Transfer (Raft) Polymerization. *Macromolecules* **2005**, *38*, 10363−10372.
(46) Cunha, A. G.; Freire, C. S.; Silvestre, A. J.; Pascoal Neto, C.; Gandini, A.; Orblin, E.; Fardim, P. Highly Hydrophobic Biopolymers Prepared by the Surface Pentafluorobenzoylation of Cellulose Substrates. *Biomacromolecules* **2007**, *8*, 1347−1352.
(47) Jin, H.; Kettunen, M.; Laiho, A.; Pynnonen, H.; Paltakari, J.; Marmur, A.; Ikkala, O.; Ras, R. H. Superhydrophobic and Super-oleophobic Nanocellulose Aerogel Membranes as Bioinspired Cargo Carriers on Water and Oil. *Langmuir* **2011**, *27*, 1930−1934.
(48) Geissler, A.; Chen, L.; Zhang, K.; Bonaccurso, E.; Biesalski, M. Superhydrophobic Surfaces Fabricated from Nano- and Micro-structured Cellulose Stearoyl Esters. *Chem. Commun.* **2013**, *49*, 4962−4964.

(49) Jones, W. R. Properties of Perfluoropolyethers for Space Applications. *Tribol. Trans.* **1995**, *38*, 557−564.
(50) Xiu, Y. H.; Zhang, S.; Yelundur, V.; Rohatgi, A.; Hess, D. W.; Wong, C. P. Superhydrophobic and Low Light Reflectivity Silicon Surfaces Fabricated by Hierarchical Etching. *Langmuir* **2008**, *24*, 10421−10426.
(51) Levkin, P. A.; Svec, F.; Frechet, J. M. J. Porous Polymer Coatings: A Versatile Approach to Superhydrophobic Surfaces. *Adv. Funct. Mater.* **2009**, *19*, 1993−1998.
(52) Park, Y. B.; Im, H.; Im, M.; Choi, Y. K. Self-Cleaning Effect of Highly Water-Repellent Microshell Structures for Solar Cell Applications. *J. Mater. Chem.* **2011**, *21*, 633−636.
(53) Chen, L. Q.; Xiao, Z. Y.; Chan, P. C. H.; Lee, Y. K. Static and Dynamic Characterization of Robust Superhydrophobic Surfaces Built from Nano-Flowers on Silicon Micro-Post Arrays. *J. Micromech. Microeng.* **2010**, *20*, 105001.
(54) de Gennes, P. G.; Brochard-Wyart, F.; Quere, D. *Capillarity and Wetting Phenomena: Drops, Bubbles, Pearls, Waves*; Springer: New York, 2004.
(55) Foote, G. B.; du Toit, P. S. Terminal Velocity of Raindrops Aloft. *J. Appl. Meteorol.* **1969**, *8*, 249−253.
(56) Barenbrug, A. W. T. *Psychrometry and Psychrometric Charts*, 3rd ed; Cape and Transvaal Printers Ltd.: Cape Town, South Africa, 1974.
(57) Boreyko, J. B.; Collier, C. P. Delayed Frost Growth on Jumping-Drop Superhydrophobic Surfaces. *ACS Nano* **2013**, *7*, 1618−1627.
(58) Mahmoudi, M.; Hosseinkhani, H.; Hosseinkhani, M.; Boutry, S.; Simchi, A.; Journeay, W. S.; Subramani, K.; Laurent, S. Magnetic Resonance Imaging Tracking of Stem Cells in Vivo Using Iron Oxide Nanoparticles as a Tool for the Advancement of Clinical Regenerative Medicine. *Chem. Rev.* **2011**, *111*, 253−280.
(59) Mahmoudi, M.; Hofmann, H.; Rothen-Rutishauser, B.; Petri-Fink, A. Assessing the in Vitro and in Vivo Toxicity of Superparamagnetic Iron Oxide Nanoparticles. *Chem. Rev.* **2012**, *112*, 2323−2338.
(60) Timonen, J. V. I; Latikka, M.; Leibler, L.; Ras, R. H. A.; Ikkala, O. Switchable Static and Dynamic Self-Assembly of Magnetic Droplets on Superhydrophobic Surfaces. *Science* **2013**, *341*, 253−257.
(61) Hermans, T. M.; Frauenrath, H.; Stellacci, F. Droplets out of Equilibrium. *Science* **2013**, *341*, 243−244.
(62) Hornig, S.; Heinze, T. Efficient Approach To Design Stable Water-Dispersible Nanoparticles of Hydrophobic Cellulose Esters. *Biomacromolecules* **2008**, *9*, 1487−1492.
(63) Vaca-Garcia, C.; Borredon, M. E.; Gaseta, A. Determination of the Degree of Substitution (DS) of Mixed Cellulose Esters by Elemental Analysis. *Cellulose* **2001**, *8*, 225−231.